A low-temperature extended X-ray absorption study of the local order in simple and complex perovskites. I. Potassium niobate

1993 J. Phys.: Condens. Matter 5 1261

(http://iopscience.iop.org/0953-8984/5/9/011)

J. Phys.: Condens. Matter 5 (1993) 1261–1270. Printed in the UK

A low-temperature extended x-ray absorption study of the local order in simple and complex perovskites: I. Potassium niobate

N de Mathan†, E Prouzet‡, E Husson†§ and H Dexpert‖

† Laboratoire de Chimie Physique du Solide, URA CNRS 453, Ecole Centrale de Paris, 92295 Chatenay-Malabry Cédex, France

‡ Laboratoire de Chimie des Solides, IMN, CNRS UMR 110, 2 rue de la Houssinière, 44072 Nantes Cédex 03, France

§ Laboratoire de Physique et Mécanique des Matériaux, ESEM, Université d'Orléans, CRPHT-CNRS, 45071 Orléans Cédex, France

‖ LURE, Université de Paris-Sud, CNRS Batiment 209 D, 91405 Orsay Cédex, France

Received 21 September 1992, in final form 25 November 1992

Abstract. An EXAFS study of potassium niobate was performed at the niobium K edge between 300 and 4.5 K. It is shown that there is no significant modification of the local environment of the niobium atoms within their oxygen octahedra with temperature. In the orthorhombic phase as well in the rhombohedral phase, each niobium is shifted by about 0.216 Å from the central position in the octahedron, along a ⟨111⟩ axis. This confirms the so called 'eight-site model' used for ferroelectric perovskites. The Nb–Nb and Nb–K distances are also considered. The complementarity of x-ray or neutron diffraction techniques sensitive to the long-range order and EXAFS spectroscopy sensitive to the local order is discussed.

1. Introduction

Structural studies by x-ray, neutron and electron diffraction, as well as HRTEM images, have shown that the nanostructure and the local order may play an important role in the diffuse ferroelectric transition in complex perovskites such as $PbMg_{1/3}Nb_{2/3}O_3$ [1]. The aim of the present work is to characterize, and to follow through an extended x-ray absorption fine structure (EXAFS) study, the evolution of the local order in $PbMg_{1/3}Nb_{2/3}O_3$, between 300 and 4.5 K, in comparison with a simple perovskite, $KNbO_3$, taken as reference. We present in this first part all the results obtained for $KNbO_3$. They extend some partial results of an in-progress study that has already been presented, on the niobium–oxygen distances between 140 and 750 K [2], in a parallel approach to our previous work [3].

Potassium niobate $KNbO_3$ undergoes successive ferroelectric transitions upon cooling from its cubic ABO_3 perovskite phase. The transitions from cubic to tetragonal, then tetragonal to orthorhombic and finally orthorhombic to rhombohedral occur at 708 K, 498 K and 263 K respectively. Numerous studies have been carried out in order to elucidate whether these transitions have a displacive or an order–disorder character. Initially, a lattice-dynamical soft-mode model was proposed [4, 5] in which components of a low-frequency cubic phonon mode become successively unstable

0953-8984/93/091261+10$07.50

and lead to a displacement of the B cation from the equilibrium position within the unit cell. These displacements are along the ⟨001⟩ direction in the tetragonal phase, the ⟨110⟩ direction in the orthorhombic phase and the ⟨111⟩ direction in the rhombohedral phase. This model is confirmed by x-ray and neutron diffraction studies: if the O octahedron is regarded as an essentially rigid unit, the B cation shift generates one Nb–O bond length in the cubic phase, three in the tetragonal and orthorhombic phases and two in the rhombohedral phase [6]. However, many studies have presented results inconsistent with this soft-mode model and the 'eight-site model' has been proposed [4,7–11]. According to this order–disorder model, in the paraelectric phase, the B cations are shifted from their ideal positions along the eight [111] cube diagonals. Below 708 K, only four of the eight sites are occupied, giving rise to a tetragonal symmetry; below 498 K, only two of the eight sites are occupied and the structure becomes orthorhombic and finally, below 263 K, only one site is occupied in the rhombohedral structure, which is alone to be ordered. Thus, according to this model, the shift of the Nb cation along the ⟨111⟩ axis generates two Nb–O bond lengths in the four structures. Therefore EXAFS at the Nb K edge should provide information about these Nb cations shifts.

2. Experimental details

2.1. EXAFS measurements

The spectra have been recorded at DCI, the French Synchrotron Laboratory LURE, using the EXAFS IV spectrometer, mounted with a two-crystal Si (331) monochromator. During the experiments, the storage ring used 1.85 GeV positrons with a 250 mA average intensity. Data were collected in transmission mode by the measurement of the beam intensities I_0 and I before and after passing through the sample, respectively, using ion chambers with argon fill gas.

Samples were prepared from 20 μm grain size powders caught in a nylon weave, then recorded at 300, 230, 100 and 4.5 K, at the Nb K edge with one second counting time per point, from 18850 to 19850 eV in 3 eV steps.

2.2. Data processing

The EXAFS analysis has been performed following a well known procedure [12] through a chain of programs written by Michalowicz [13]. The absorption spectra studied have been obtained by averaging three experimental spectra by a cumulative approach $\mu(E) = \ln(\sum I_0/\sum I)$. The EXAFS signal $\chi(E)$ is equal to $[\mu(E) - \mu_1(E)]/[\mu_1(E) - \mu_0(E)]$ where $\mu(E)$ is the observed absorption, $\mu_1(E)$ the atomic absorption and $\mu_0(E)$ the sample absorption. This last parameter has been developed from an analytical expression using the formula of Lengeler and Eisenberger [14]. The atomic absorption coefficient $\mu_1(E)$ was approximated by a fifth-degree polynomial expression from 19008 to 19850 eV. The EXAFS contribution was calculated between 19010 and 19850 eV with E_0 taken equal to the energy at half the edge jump, 18986 eV.

A Kaiser window ($\tau = 3.5$) was then applied to the $k^n\chi(k)$ ($n = 1$ or 2 for the O and Nb shells respectively) weighted data before Fourier transforming from $k = 2.8$ up to 14.0 Å^{-1} ($E \simeq 30$–750 eV). All the moduli curves of the Fourier transforms are uncorrected for phase shift.

The wave vector of the photoelectron ejected from the absorbing atom with kinetic energy $E_c = E - E_0 = h\nu - E_0$ is

$$k = \sqrt{(8\pi^2 m_e/h^2)(E - E_0)}.$$

The various shells have been first extracted by a back Fourier transform including a removal of the Kaiser window contribution, then studied through a fitting procedure with simplex and gradient methods using the MINUIT program [15] and Teo and Lee's [16] tabulated amplitudes and phase shifts. For all the fits, the number of variables was chosen so as to not pass beyond $(N_{ind} - 1)$ with N_{ind} defined as the number of independent variables and equal to $(2\Delta k \Delta R/\pi)$, Δk being the size of the fitted EXAFS spectra ($\Delta k = \Delta k_{max} - \Delta k_{min}$) and ΔR the size of the back Fourier transformed window.

The back Fourier transformed contributions of each of the various shells have been analysed through the classical EXAFS formula based on the plane wave single-scattering theory, expressed by the equation

$$k\chi(k) = -S_0^2 \sum_i \frac{N_i}{R_i^2} \exp(-2k^2\sigma_i^2) \exp(-2R_i\Gamma/k) f_i(\pi, k) \sin[2kR_i + \Phi_i(k)].$$

S_0 is a scale factor which translated the fact that just a fraction of the photoelectrons ejected is taking part in the EXAFS phenomenon; N_i is the number of neighbours at distance R_i from the absorbing atom; $\Gamma = k/\lambda$ where λ is the mean free path of the photoelectron; $f_i(\pi, k)$ and $\Phi_i(k)$ are respectively the amplitude and phase shift functions characteristic of the ejection of an electron from the central atom and its backscattering by the neighbours; σ_i is a damping coefficient due to thermal motion and distance distribution in the shell, i.e. the Debye–Waller factor. When theoretical amplitude and phase shift files are used, S_0 and Γ can be considered as agreement factors. Therefore they are not allowed to vary for the whole series of samples. The reliability of the fit is determined by the error factor ρ:

$$\rho = \sum_k k^{2q}[k\chi_{exp}(k) - k\chi_{theo}(k)]^2 \Big/ \sum_k k^{2q}[k\chi_{exp}(k)]^2.$$

The q parameter has been taken as equal to 0.5 for this study.

3. Results and discussion

Figure 1 compares the moduli of the Fourier transforms of EXAFS spectra at temperatures 300, 230, 100 and 4.5 K. The first two peaks correspond to the octahedral O environment. The next peak is due to the first eight K neighbours; this was not fitted because of the dispersion of the Nb–K distances: 3.39, 3.45, 3.51 and 3.57 Å [6]; then the peak of the Nb atoms in the six closest octahedra is observed. The contribution of the second O shell (12 O at 4.32, 4.44, 4.55 and 4.66 Å) that should arise near 4.0 Å, does not appear because of (i) the dispersion of the distances and (ii) the weak O back scattering amplitude. The other peaks observed are due to the other Nb shells.

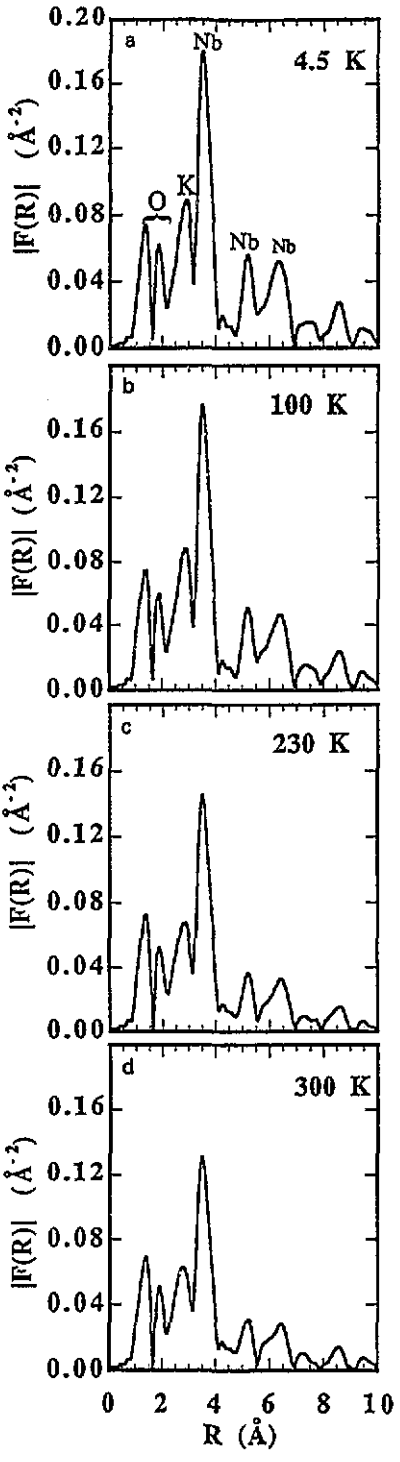

Figure 1. Moduli of the Fourier transform of the $k\chi(k)$ data at the Nb K edge EXAFS spectra for the 300, 230, 100 and 4.5 K samples (uncorrected for phase shift). The radial distribution function exhibits the two O shells, the K shell, then the successive Nb shells corresponding to the Nb–Nb distances a, $a\sqrt{2}$, $a\sqrt{3}$, $2a$, $a\sqrt{5}$ and $a\sqrt{6}$ (a: cell parameter).

3.1. The oxygen shell

All the Fourier transform moduli of the EXAFS spectra exhibit two peaks that can be

attributed to the O neighbours; they have virtually the same profiles and the same intensities at all the temperatures in contrast to other peaks for which an increased intensity is observed when the temperature is lowered. This shows that two types of Nb–O distance exist in the rhombohedral phase as well as in the orthorhombic phase. The fits were performed between 2.8 and 14.0 $Å^{-1}$ on $k\chi(k)$ EXAFS spectra resulting from an inverse Fourier transform taken from 1.07 to 2.10 Å. Taking into account that the amplitude and phase shift are theoretical files, we firstly refined $\Gamma(\Gamma_1 = \Gamma_2 = 0.91)$ and $S_0 = 0.8$, then the other parameters were refined.

First we let N_i and σ_i vary together (figure 2). We cannot see any obvious variation of these parameters with the temperature: N_1 and N_2 remain close to three and there are weak variations of σ_1 and σ_2 from 4.5 to 300 K. N_2 is larger than N_1, and σ_2 is larger than σ_1; it is well known that an increase of the number of neighbours increases the EXAFS signal intensity, in contrast to an increase of the Debye–Waller factor. This is why we can assume that the (N_1, σ_1) and (N_2, σ_2) couples reflect the same structural situation, according to a (3+3) neighbours model.

Table 1. Results of the fits for the two O coordination shells. N_i and R_i represent respectively the number of O atoms and the distances Nb–O. σ_i and ΔE_i are the Debye–Waller factor and the energy shift versus the experimental K Nb edge. ρ is the error factor. The fitting is performed with Teo and Lee's tabulated amplitude and phase shift files; S_0 (the scale factor) and Γ ($\Gamma = k/\lambda$ where λ is the electronic mean free path) are respectively fixed to 0.8 and 0.91; σ_i and ΔE_i are absolute values with reference to the theoretical spectrum. The R_{O1} and R_{O2} values are consistent with those obtained from neutron diffraction structural determination and the small evolution of σ_i shows that the O octahedron is weakly affected by the thermal effect and the orthorhombic to rhombohedral transition.

	300 K orthorhombic	230 K rhombohedral	100 K rhombohedral	4.5 K rhombohedral	230 K crystallographic data from [6]
N_{O1} (fixed)	(3)	(3)	(3)	(3)	3
R_{O1} (Å)	1.89	1.89	1.89	1.89	1.89
σ_{O1} (Å)	0.067	0.061	0.059	0.059	
ΔE^0_{O1} (eV)	10.6	13.7	13.4	13.4	
N_{O2} (fixed)	(3)	(3)	(3)	(3)	3
R_{O2} (Å)	2.15	2.15	2.15	2.15	2.14
σ_{O2} (Å)	0.075	0.069	0.059	0.059	
ΔE^0_{O2} (eV)	9.8	13.0	12.9	12.9	
ρ (%)	3.8	1.9	1.8	1.8	

After this first simulation, N_1 and N_2 parameters were fixed as three in order to follow the evolution of the σ_i parameters with temperature. The results are summarized in table 1. The Nb–O distances R_1 and R_2 are consistent with the values calculated from neutron diffraction structural determination, respectively 1.89 and 2.14 Å [6]. The Debye–Waller factor is originated from both static and thermal disorder. At 4.5 K, the latter is obviously very close to zero. Thus, the value of $\sigma_{4.5\ K}$ represents the static disorder assuming a Gaussian pair distribution around the average position. There is a very small evolution of these parameters with temperature: the oxygen octahedron is weakly affected by the thermal effect and there is no structural modification of this site with the orthorhombic to rhombohedral transition. Figure 3 exhibits the simulated and experimental EXAFS and Fourier

Table 2. Results of the fits performed, firstly for the Nb coordination shell, second for the outer shells (second and third Nb shells and second K shell). N_i and R_i represent respectively the number of backscattering atoms and their distances from Nb. σ_i and ΔE_i are the Debye–Waller factor and the energy shift versus the experimental K Nb edge. ρ is the error factor. The fitting is performed with Teo and Lee's tabulated amplitude and phase shift files; S_0 (the scale factor) and Γ ($\Gamma = k/\lambda$ where λ is the electronic mean free path) are respectively fixed to 0.9 and 0.47; σ_i and ΔE_i are absolute values with reference to the theoretical spectrum.

	300 K orthorhombic	230 K rhombohedral	100 K rhombohedral	4.5 K rhombohedral	230 K crystallographic data from [6]
N_{Nb1} (fixed)	(6)	(6)	(6)	(6)	6
R_{Nb1} (Å)	4.03	4.03	4.03	4.03	4.016
σ_{Nb1} (Å)	0.051	0.045	0.032	0.024	
ΔE^0_{Nb1} (eV)	−28.2	−24.5	−24.5	−26.1	
ρ (%)	2.7	3.5	3.4	1.9	
N_{Nb2} (fixed)	(12)	(12)	(12)	(12)	12
R_{Nb2} (Å)	5.67	5.67	5.67	5.67	5.679
σ_{Nb2} (Å)	0.103	0.095	0.081	0.077	
ΔE^0_{Nb2} (eV)	−16.6	−12.0	−11.7	−14.4	
N_K (fixed)	(24)	(24)	(24)	(24)	24
R_K (Å)	6.50	6.52	6.58	6.64	Six values from:
σ_K (Å)	0.150	0.144	0.130	0.125	6.58–6.74
ΔE^0_K (eV)	−20.0	−15.3	−13.0	−13.0	
N_{Nb3} (fixed)	(8)	(8)	(8)	(8)	8
R_{Nb3} (Å)	6.96	6.97	6.97	6.97	6.955
σ_{Nb3} (Å)	0.071	0.060	0.043	0.037	
ΔE^0_{Nb3} (eV)	−28.7	−23.7	−22.9	−24.8	
ρ (%)	7.0	5.6	4.6	5.0	

transform (modulus and imaginary part) spectra; in addition to the low value of the error factor, this comparison confirms the fact that the model describing three O atoms in each shell has a real physical meaning.

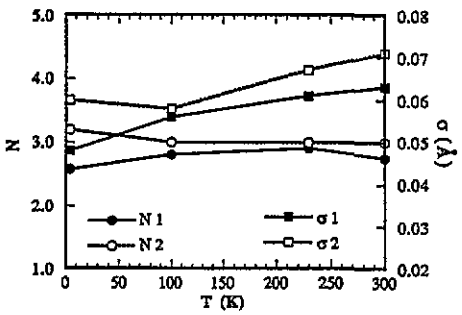

Figure 2. Evolution of the number of neighbours (N) and the Debye–Waller factors (σ) versus the temperture, in the case of simulations for which all the N_i and σ_i are allowed to vary freely. N_1 and N_2 remain close to three and the variations of σ_1 and σ_2 from 4.5 to 300 K are not too strong according to a (3 + 3) neighbours model.

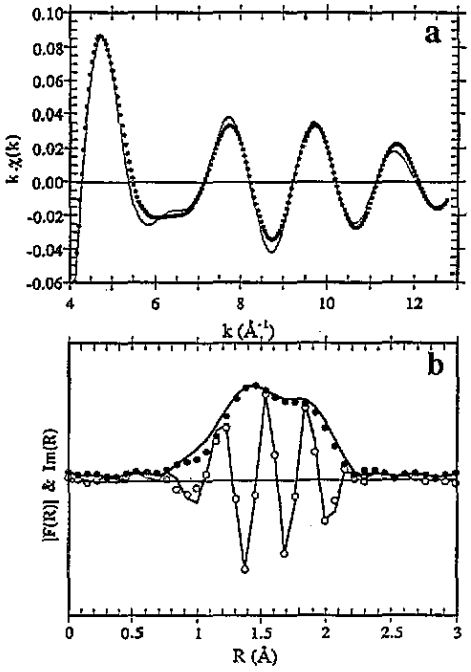

Figure 3. Simulated spectra for the two O shells of the $KNbO_3$ (4.5 K) $k\chi(k)$ EXAFS spectrum: (*a*) EXAFS spectrum (——, experimental; ●, calculated); (*b*) Fourier transform (——, experimental modulus and imaginary part; ●, calculated modulus; O, calculated imaginary part).

The similarity of the EXAFS spectra of the O shells (figure 4) and the weak evolution of the values of the Debye–Waller factor show that there is no significant modification of the local environment of the Nb atoms within their O octahedra with temperature. Each Nb is shifted from the central position in the octahedron, along a ⟨111⟩ axis, closer to three O atoms (1.89 Å) and further from three others (2.14 Å); this shift is equal to 0.126 Å.

Table 3. Distribution of neighbours in the various shells around Nb, deduced from the EXAFS analysis. Nb is shifted by 0.126 Å from the centre of its O octahedral site, along a ⟨111⟩ axis. The Nb–K distance increases progressively from 6.50 Å (300 K) to 6.64 Å (4.5 K).

	Number of neighbours	*R* (Å)
O	3	1.89
O	3	2.15
Nb	6	4.03
Nb	12	5.67
K	24	6.50 (300 K)–6.64 (4.5 K)
Nb	8	6.97

3.2. The first niobium shell and the outer shells

For the first niobium shell, fits have been performed between 3.2 and 14.7 $Å^{-1}$ on

$k\chi(k)$ EXAFS spectra extracted by a back Fourier transform taken from 3.1 to 4.2 Å ($N_{ind} = 7$) (figure 5). For the outer shells (second and third Nb and second K shells), they have been simulated with the same $k\chi(k)$ EXAFS spectra from a 4.6–6.8 Å back Fourier transform ($N_{ind} = 16$) (figure 6). Taking into account that the amplitude and phase shift are theoretical files, we firstly refined Γ ($\Gamma_i = 0.47$) and $S_0 = 0.9$, then the other parameters were adjusted with the numbers of neighbours for each shell set equal to the known values deduced from the structure. The results are given in table 2.

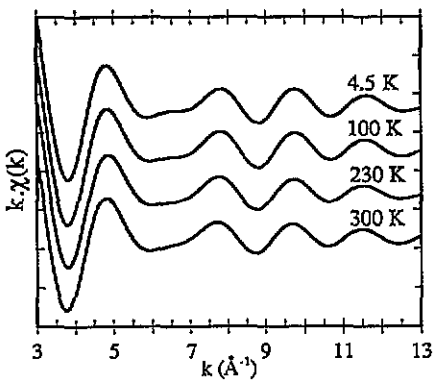

Figure 4. Comparison of the $KNbO_3$ $k\chi(k)$ EXAFS spectra at 300, 230, 100 and 4.5 K. Their similarity shows that the modifications of the local order around the Nb within the O octahedra are very weak.

All the Nb–Nb distances remain fairly constant with temperature and close to those obtained from the crystallographic data. In the orthorhombic phase, the different Nb–Nb(1) distances (statistically 0.5 d_1 at 3.775 Å, 3 d_2 at 4.015 Å, 2 d_3 at 4.022 Å and 0.5 d_4 at 4.256 Å) could not be observed, due to their dispersion and to the small difference between d_2 and d_3 lengths.

The Nb–K distances shorten linearly from 4.5 K (6.64 Å) to 300 K (6.50 Å). For a calculated EXAFS spectrum, a variation of ΔE^0 can be partially compensated by a backscatter-absorber distance shift. In this case, the decrease of ΔE^0—that leads to an EXAFS signal phase decrease, mainly at the beginning of the spectrum—should be compensated by a lengthening of the calculated distance in contrast to what is observed. Therefore taking into account the relative variation of ΔE^0 and R parameters with temperature, this result cannot be a fitting artifact. Moreover, our trials to fit the 300 K spectrum by fixing R to 6.64 Å, letting ΔE^0 and σ vary, did not lead to good agreement between the experimental and simulated spectra. The shortening of the Nb–K distances when the temperature increases is in good agreement with the neutron diffraction results [6] showing a decrease of these distances from 540 K in the tetragonal phase down to 230 K in the rhombohedral phase. Thus, these distances should continue to decrease with temperature in the rhombohedral phase down to 4 K.

4. Conclusion

Table 3 summarizes the whole set of distances found through this EXAFS analysis. It

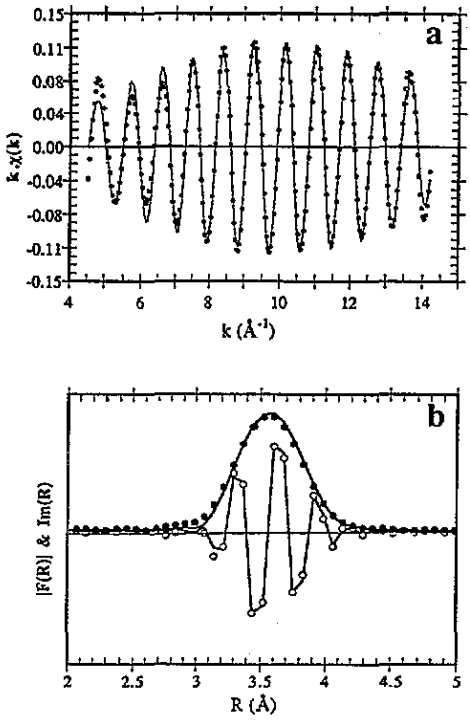

Figure 5. Simulated spectra for the first niobium shell of the $KNbO_3$ (4.5 K) $k\chi(k)$ EXAFS spectrum: (*a*) EXAFS spectrum (——, experimental; ●, calculated); (*b*) Fourier transform (——, experimental modulus and imaginary part; ●, calculated modulus; ○, calculated imaginary part).

can be seen that in the rhombohedral phase, the Nb shift along one [111] direction of the basis cube within its O octahedron, considered as rigid, originates three short Nb–O bonds and three longer ones. In this case, the local position detected by EXAFS and the average position determined by x-ray or neutron diffraction is the same. In contrast, in the orthorhombic phase, the Nb cations statistically shift along two possible [111] directions (figure 7). Thus, at short range, in a given octahedron, the Nb cation shift is identical to that of the rhombohedral phase, whereas the long-range average position of the Nb appears like a shift along a [110] axis.

This study gives direct confirmation of the 'eight-site model' [7,8] and thus the order–disorder character of the phase transitions in ferroelectric perovskites such as $KNbO_3$. It shows also the complementarity of structural methods sensitive to the long-range order (x-ray and neutron diffraction) to those sensitive to the local order: among these EXAFS is a powerful method.

Supplementary material available

A document including software description, raw data, figures of the spectra for each step of the calculation, details of fitting results and final maps of χ^2 versus parameters of refinement, is available from the authors (50 pages).

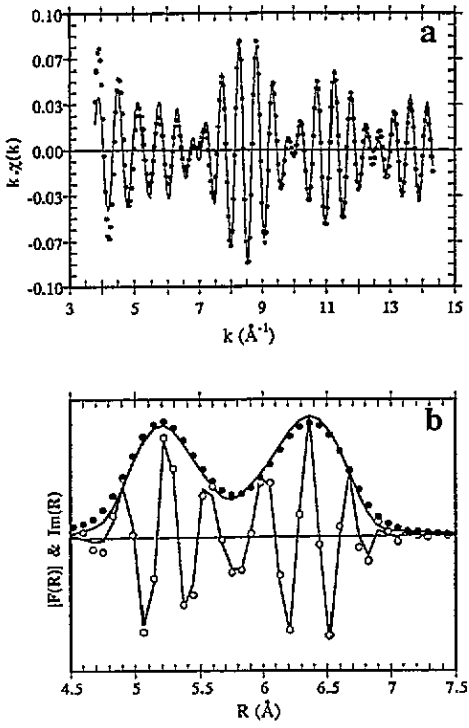

Figure 6. Simulated spectra for the outer shells of the $KNbO_3$ (4.5 K) $k\chi(k)$ EXAFS spectrum: (*a*) EXAFS spectrum (——, experimental; ●, calculated); (*b*) Fourier transform (——, experimental modulus and imaginary part; ●, calculated modulus; ○, calculated imaginary part).

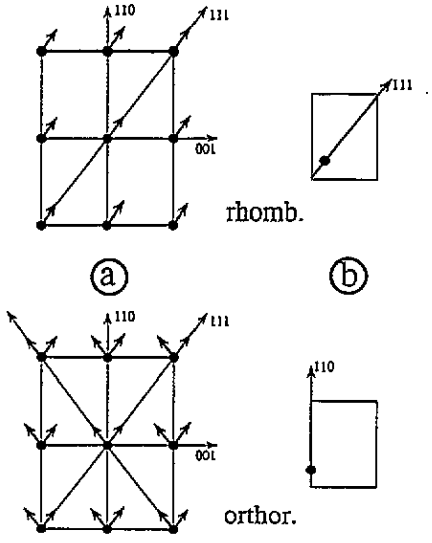

Figure 7. (*a*) Nb atom shifts in the rhombohedral and orthorhombic phases of $KNbO_3$; (*b*) Nb atom average position determined by x-ray and neutron diffraction.

References

[1] de Mathan N, Husson E and Morell A 1992 *Mater. Res. Bull.* **27** 867
[2] Kim K H, Elam W T and Skelton E F 1990 *Mater. Res. Soc. Symp. Proc.* **172** 291
Bell M I, Kim K H and Elam W T 1991 *Ferroelectrics* **120** 103
[3] de Mathan N 1991 *Thesis* Ecole Centrale de Paris, France
[4] Cochran W 1960 *Adv. Phys.* **9** 387
[5] Cochran W 1961 *Adv. Phys.* **10** 401
[6] Hewat A W 1973 *J. Phys. C: Solid State Phys.* **6** 2559
[7] Comes R, Lambert M and Guinier A 1968 *Solid State Commun.* **6** 715
[8] Comes R, Lambert M and Guinier A 1970 *Acta Crystallogr.* A **26** 244
[9] Itoh K, Zeng L Z, Nakamura E and Mishima N 1985 *Ferroelectrics* **63** 29
[10] Edwardson P J 1989 *Phys. Rev. Lett.* **63** 55
[11] Sokoloff J P, Chase L L and Rytz D 1988 *Phys. Rev.* B **38** 597
[12] Lyttle F W, Sayers D E and Stern E A 1975 *Phys. Rev.* B **11** 4825
Stern E A, Sayers D E and Lyttle F W 1975 *Phys. Rev.* B **11** 4836
[13] Michalowicz A 1991 *Logiciels pour la Chimie* (Paris: Société Française de Chimie) p 102
[14] Lengeler B and Eisenberger P 1980 *Phys. Rev.* B **21** 4507
[15] James F and Roos M 1976 MINUIT CERN computing centre program library *CERNID internal report* 75/20
[16] Teo B K and Lee P A 1979 *J. Am. Chem. Soc.* **101** 2815